Hindawi
Geofluids
Volume 2022, Article ID 7209176, 12 pages
https://doi.org/10.1155/2022/7209176

Research Article

Multiscale Investigations of Overtopping Erosion in Reinforced Tailings Dam Induced by Mud-Water Mixture Overflow

Meibao Chen,[1] Xiaofei Jing,[1] Xiaohua Liu,[1] Xuewei Huang,[1] and Wen Nie[2]

[1]*School of Safety Engineering, Chongqing University of Science and Technology, Chongqing 401331, China*
[2]*Key Laboratory of Safety and Health for Metal Mines, Maanshan 243000, China*

Correspondence should be addressed to Xiaofei Jing; xfjing@cqust.edu.cn and Xiaohua Liu; 2021207059@cqust.edu.cn

Received 19 August 2022; Accepted 21 September 2022; Published 10 October 2022

Academic Editor: Zhenlong Song

The overtopping failure that occurred to the reinforced tailings dam has led to devastating catastrophes, including severe environmental disasters as well as tragedy in terms of any loss of properties and life. To study the feature of overtopping erosion for the reinforced fine-grained tailings dam induced by mud-water mixture overflow, the red mud concentration of overflow, the erosion depths and erosion rate have been consistently detected and recorded by a series of physical model tests. This investigation conclusively showed that the red mud concentration for flooding over the dam slope had a nonlinear trend of first becoming larger, subsequently decreasing with the time going on in the process of tailing dam overtopping; the maximum red mud concentration achieved 19.0%. The erosion on the dam slope was shaped like a trumpet. The red mud concentration of the mud-water mixture flow affected the erosion depth significantly. The hydraulic tests simulating erosion behaviour in the reinforced fine-grained tailings were carried out with different red mud concentrations (0%, 10%, and 20%). For the mud-water mixture flow in a red mud concentration of 20%, the final erosion depth exhibited a ladder shape from the front to the trailing end (dam toe) of the tailings sample. The final erosion depths were 1.56 cm, 0.9 cm, and 0.55 cm at the front, middle, and trailing end, respectively. With the red mud concentration decreasing, the final erosion depth at the front of the tailings sample reduced significantly while increasing at the trailing end. This study brought more scientific insights into the overtopping erosion process to the reinforced fine-grained tailings dam triggered by the mud-water mixture flow at multiscale.

1. Introduction

Tailings reservoir has been one of mineral production's three main engineering projects. Also, it has brought a massive danger for artificially built mudslides with high potential energy, i.e., dam failure is at risk. Amongst ninety-three kinds of accidents and public hazards worldwide, tailings pond accidents ranked eighteenth [1].

Several failures of tailings impoundments have occurred over the past decades for a diversity of reasons, which include liquefaction of residual tailings, internal erosion (suffusion), contact erosion, overtopping erosion of dams, or excessive seeping flow that can create breaches [2–6]. Amongst those types of erosions, overtop flooding was identified as the primary cause of failure in tailings dams [7]. For example, a village downstream was destroyed in a tailings pond collapse accident in Bulgaria's Mir mine, resulting in a casualty of 488 people [8]. There were 281 people killed in a severe tailings dam break at Xinta Mining Company, Shanxi Province, China [9]. To reduce the number of such accidents, more and more attention has been paid to the safe operation of tailings dams worldwide. The reasons for the destruction of the tailings reservoir are complex and even caused by various factors. Many scholars have studied and analysed the mechanism of tailings dam erosion, and many achievements have been made.

Most experts and scholars have conducted physical modelling, mathematical modelling, and other methods to investigate possible causes of overtopping erosion in tailings dams. For example, Yao [10] found that the shear strength of tailing could be seen as a dominating parameter for analysing the erosion sensitivity of tailings dams using their custom-designed testing device. Beforehand, Yang et al. [11] also simulated the destruction process of the

overtopping dam failure when encountering a flood peak through their specific-designed tests in a flume. To study the effects of water flow and tailing sand on the downstream and dam toe after dam failure, Chen et al. [12] constructed a three-dimensional hydrodynamic dam failure model; they further carried out the transport calculation of tailing and the verification of the modelling accuracy with a series of collapse tests in a flume. A decade ago, Hancock [13] already proposed a landscape evolution model that generalised the erosion process inside the dam body and the relationship between it and its influencing factors through visual modelling. Recently, Li et al. [14] analysed the spatial evolution of mud and rock flow during the tailing dam collapsing; they consequentially established a three-dimensional safety-monitoring and early-warning system, which has been mainly applied for detecting the actual topography and assessing the backfill status for tailings dams.

These investigations of dam overtopping failure have been recently conducted with additional consideration of dam reinforcement. Based on the theory of similarity and the principle of rupture erosion, Jing et al. [15] physically modelled the overtopping-induced failure of tailing dams under different reinforcing conditions; e.g., they specifically analysed the influence of rib density (reinforcement density) on the overtopping failure of tailings dams. Meanwhile, Zhao et al. [16] also carried out many geophysical modelling works in physically simulating the flooding-induced overtopping failure of the reinforced tailings dam; an in-depth analysis of the evolution law and failure mode revealed the geogrid's blocking effects on the overtopping failure of tailings dams. Later, intending to increase the height and capacity of tailings reservoirs, Gao et al. [17] attempted to apply the concept of reinforced soil in geotechnical engineering in designing the tailing dam for a tailing reservoir.

With downscaling from the large scale for the overall tailing dam, the mechanism of overtopping erosion could be simplified and thereby treated as an issue of sedimentation transport at the local scale. For instance, Bahmanpouri et al. [18] experimentally and numerically studied the erodible layer's particle transport and morphological evolution caused by the overtopping flow. They also investigated the effects of three compacting conditions at the dam shoulder and toe. Beforehand, Petkovšek et al. [19] extended the dual-fluid (water and tailings flow) model to the EMBREA dam failure model. At a much earlier stage, Bagnold [20] adopted a hydraulic test with a lightweight sand flume to observe the turbulence intensity variation in water flow during an erosion process, eventually concluding that the turbulence intensity significantly decreased by gradually increasing the sand content under a hydraulic condition of constant head. Later, for further studying the changes in turbulence intensity before and after adding fine sediment, Bruhl and Kazanskij [21] set up a sedimentation transport experiment in a horizontal column test (diameter of 100 mm) with a uniform coarse sand (median particle size of 1 mm); the experimental results showed that the turbulence intensity was significantly reduced after the sediments were more accumulated in thickness by adding more fine particles. Shvidchenko and Pender [22] conducted an experimental study on the initial motion of coarse uniform sediments, showing that the critical flow conditions for uniform sediment motion depended not only on particle size but also on the ratio of flow depth to particle size and derived a Shields plot of critical stress, grain Reynolds number, and depth and particle size ratio. Torfs et al. [23] studied the effects of sand on mud settlement and consolidation in many door experiments. They used the experimental results to develop modelling guidelines for sedimentation and consolidation of mud and sand mixtures.

Even though overtopping failures to both the reinforced and unreinforced tailing dams have been separately explored and investigated over the last few decades, there has been minor research effort devoted to studying the effect of tailings concentration of the overflow on the erosion process during an overtopping failure. With an additional consideration of the influence of overflow, the overtopping erosion features are still worth investigating. Conducting such an investigation will contribute to constructing a novel and advanced framework of theory for modelling and predicting the flooding-induced overtopping failure of tailing dams. Therefore, the research objective of this study was to analyse the features of overtopping erosion by considering the red mud (tailings) concentration of mud-water mixture flow during a flooding process. This work was achieved by applying a custom-designed Reinforced Tailings Incipient Motion Test System (RTIMTS), which consisted of a glass flume, a sample tank, a water pump, and an electromagnetic flowmeter. Furthermore, a numerical model for erosion estimation and prediction in consideration of the red mud concentration of the flooding mixtures was newly proposed and fully developed using a commercial software package (FLOW-3D). This numerical model can subsequently be applied to estimating the gully depth of the erosion process partially influenced by the red mud concentration of flooding mixtures. Besides, this study provided comprehensive datasets to facilitate and improve the risk estimation of the reinforced tailing dames when the flooding-induced overtopping failure was encountered.

2. Experiments on the Overtopping Erosion in Reinforced Tailing Dam at the Macroscale

2.1. Experimental Facilities. Tailing Dam Overtopping Failure Test System (TDOFTS) consisted of a testing hydraulic flume, water injection system, and monitoring system (see Figure 1). The flume was used as the testing area of the stacked tailing dam. The hydraulic injection system mainly consists of a water tank, water valve, pump, and water supplying pipeline, which simulated the upstream confluence flow that the modelled tailings dam encountered. The recording camera (provided by SONY in settings of the resolution of 1920 x 1080 and 50 frames per second, Beijing city, the People's Republic of China) was selected as the visually recording equipment for this dam damage monitoring system (DDMS). The vertical and horizontal dimensions of the modelled tailing dam with specific locations of preembedded reinforcements in geogrid are schematically depicted in Figure 2.

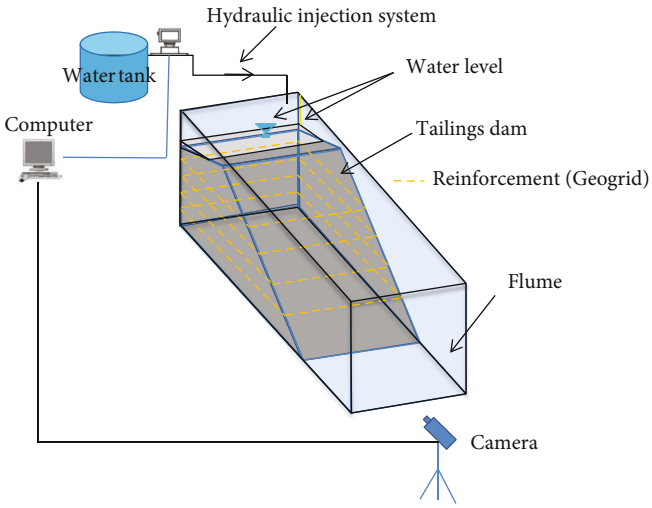

Figure 1: Tailings Dam Overtopping Failure Model Test System (TDOFMTS).

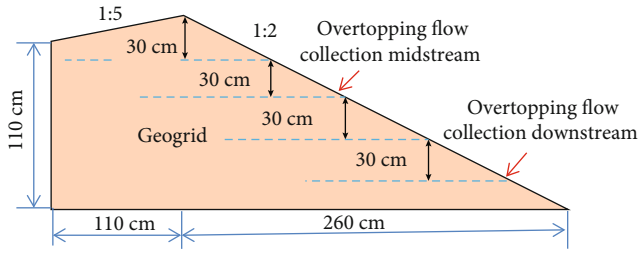

Figure 2: The schematic diagram of the geogrid.

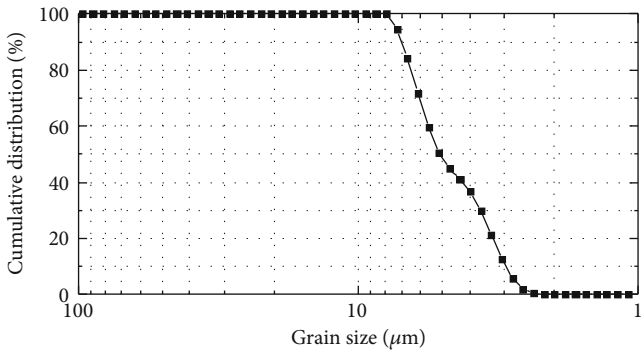

Figure 3: Grain size distribution (GSD) of the selected red mud sample.

Table 1: Fundamental properties of the applied geogrid.

Type	Grid size (mm)		Tensile strength ($kN.m^{-1}$)		Elongation (%)
	Vertical	Horizontal	Vertical	Horizontal	
JT1101	25	25	6.5	6.5	12.7

2.2. Materials and Experimental Procedures. The red mud material utilised in all tests was collected from a tailings disposal where is located in Chongqing city, the People's Republic of China. Figure 3 shows the selected red mud's grain size distribution (GSD). The particle size analysis showed the grain median size d50 = 5.1 μm; the other characteristic sizes d10 = 2.9 μm, d30 = 3.6 μm, d60 = 5.6 μm, and d90 = 7.0 μm; and the coefficient of uniformity Cu = 1.76 and the coefficient of curvature Cc = 0.79. Regarding the aforementioned parameters and coefficients of particle analysis, this red mud material could be classified as fine-grained silty tailings according to the natural standard of China (GB/T 50123-2019).

Geogrid was adopted as the reinforcing material for these physical modelling works in geotechnics [24]. The mechanical properties of the applied geogrid with its vertical and horizontal dimensions are listed in Table 1.

In accordance with the theory of similarity, a model of the tailing dam ought to be built firstly, followed by a gradual upward layered compaction method for mounding the tailing dam model. The tailing dam model (see the design in Figure 2) was tested after laying all geogrids horizontally inside the modelled tailing dam. Then, the water injection system was switched to continuously fill the model tailings dam with water at 0.5 L/s. When the water level in the reservoir was raised above the dam top until overflow, the overtopping failure could be initialised and subsequently observed. Finally, the water continuously flowed over the dam top until the modelled dam totally failed.

In the overtopping process, ten beakers, each with a capacity of 500 mL, were used to collect the overtopping discharge every 120 s at the locations of midstream and downstream of the modelled dam. At the end of the test, the mass of these ten discharging samples was weighed using a digital scale, followed by a reweighing after oven-drying for 48 hours. The red mud concentrations were obtained by calculating the ratio of the mass of the discharged red mud to the mass of the discharged overtopping flow.

2.3. Results and Discussion. This test focused on observing the red mud concentration of overtopping flow along the top surface of the dam slope. Figure 4 shows that when the test was carried out at 60 s since the video recording, the

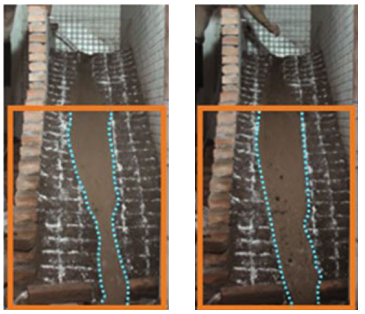

60 s 120 s

(a) 60 s (b) 120 s

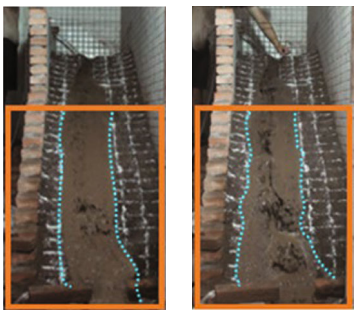

180 s 240 s

(c) 180 s (d) 240 s

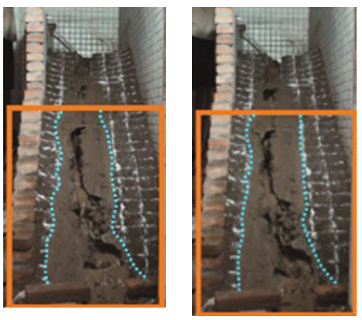

300 s 360 s

(e) 300 s (f) 360 s

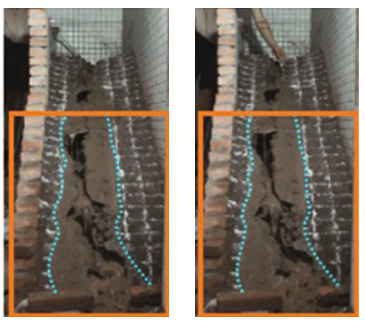

420 s 480 s

(g) 420 s (h) 480 s

Figure 4: Continued.

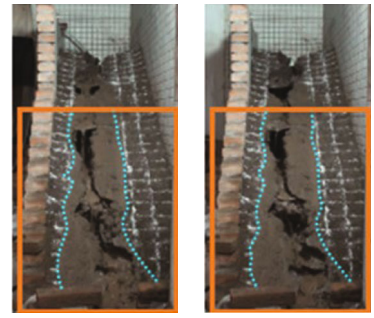

(i) 540 s (j) 600 s

Figure 4: The demonstrations of the overtopping erosion on the tailing dam models with the reinforcement of geogrids.

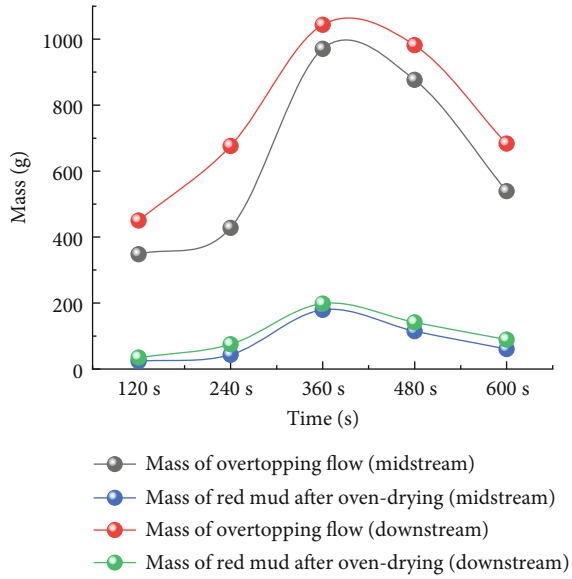

Figure 5: The mass of overtopping flow samples.

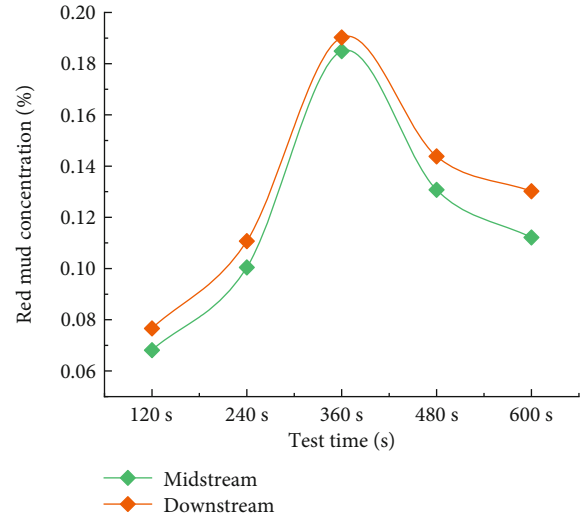

Figure 6: Red mud concentrations at the dam midstream and downstream (middle of slope and dam toe).

Table 2: Red mud concentrations of the flow in the midstream and downstream.

Time (s)	Red mud concentration at midstream	Red mud concentration at downstream
120	6.8%	7.6%
240	10.0%	11.0%
360	18.4%	19.0%
480	13.0%	14.3%
600	11.2%	13.0%

gullies began to appear on the dam slope. At 240 s, a gully (32 cm ×6 cm, width×depth) was generated in the middle slope of the tailings dam. At 600 s, the test was finished; in the meantime, the geogrids were exposed, and a ladder shape of the tailing dam model was exhibited. In the overtopping process, the overtopping flow was collected at the midstream and downstream every 120 s. As a result, the red mud concentration of the overtopping flow was obtained and plotted against time in Figure 5.

Figures 4 and 5 show that the red mud content in the overtopping flow was minimal when the test was carried out to 120 s, indicating that fewer red mud particles were washed away. At 240 s, when the gully was formed gradually on the slope, the erosion began to intensify, and the red mud content in the flow increased. At 360 s, the degree of erosion was the most intense, and then the degree of erosion gradually decreased. During the same period, the weight of the red mud downstream was higher than that in the midstream.

The red mud concentrations (as the percentage (%) by mass/mass) of the overtopping flow at the dam midstream and dam toe (downstream) are shown in Table 2. The historical variation of the red mud concentrations in the overflow is plotted in Figure 6. It was straightforward to find that the red mud concentration of this erosion test ranged from 6.8% to 19.0%. The red mud concentration increased with time to a maximum concentration at 360 s, after which it decreased; the maximum values of red mud concentrations at midstream and downstream were 18.4% and 19.0%, respectively.

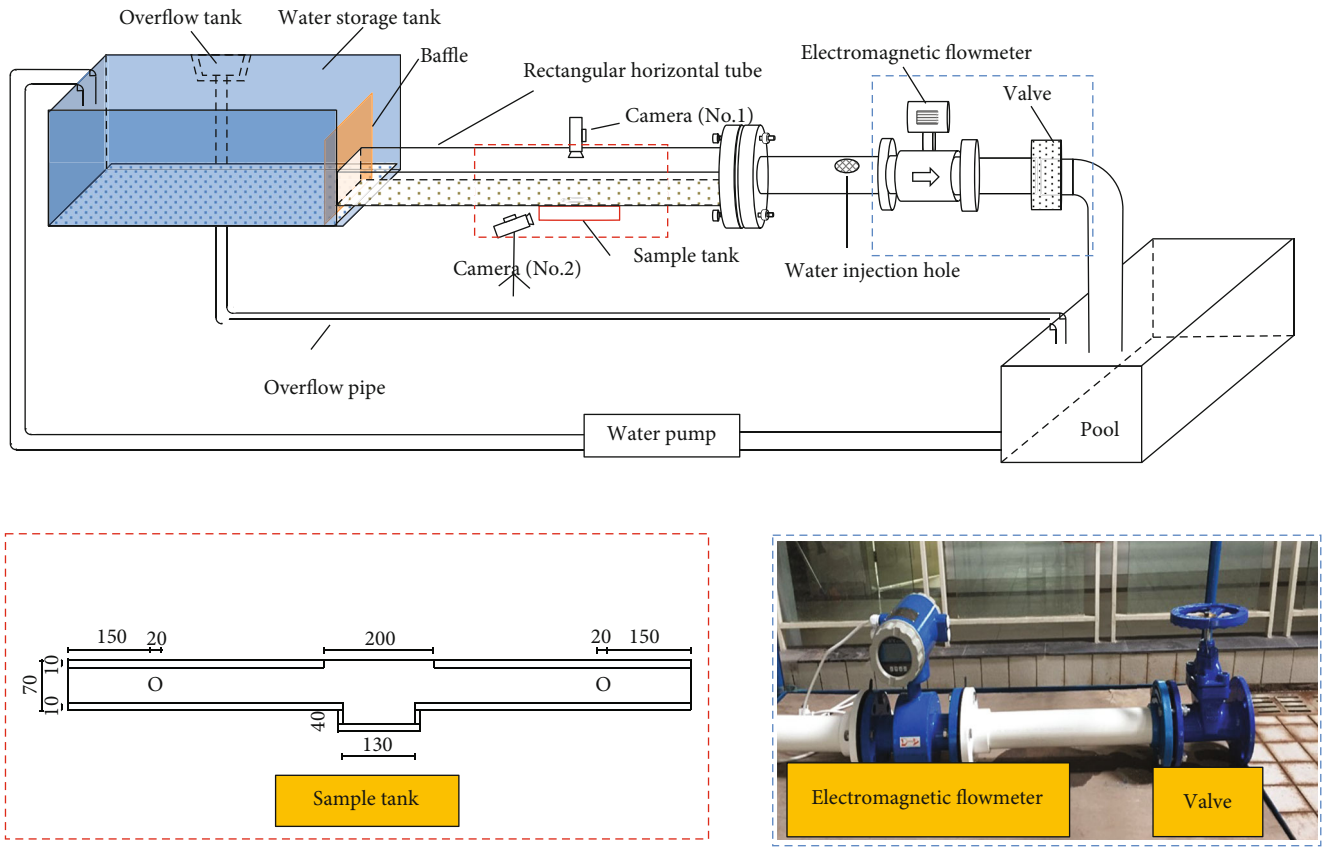

Figure 7: Reinforced tailings preset in the sample tank of the sediment incipient motion test system.

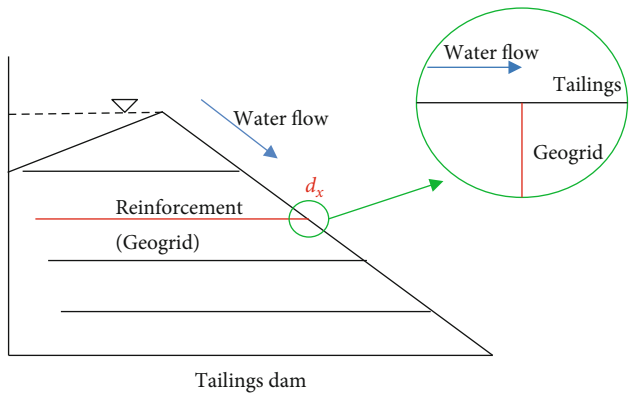

Figure 8: The layout of the reinforcements (i.e., geogrids) in the fine-grained tailing dam model.

3. Erosion Test of Reinforced Fine-Grained Tailings at the Local Scale

3.1. Experimental Facilities. The overall design of the device is shown in Figure 7. The specific design ideas of the device are as follows: (1) A horizontal-laid rectangular tube was made of transparent acrylic. Its dimensions in three directions were 180 cm in length, 8 cm in width, and 5 cm in height, respectively. The interior surface of the tube was relatively smooth, so the influence of hydraulic roughness could be ignored. (2) The groove so-defined as the sample tank had dimensions of 13 cm ×5 cm ×4 cm (length×width×height). (3) A glass tank (length × width × height =2.0 m ×0.6 m ×0.6 m) was manufactured to build up a water-recycling system, which could be seen as water storage (the pool at the bottom) for recycling the discharged water from the outlet back to the constant head tank (the water storage tank with overflow at the top). (4) The water pump was used as a water-recycling power unit with a power of 1.5 kW, a flow rate of 40 m^3/h, a total water head lift of 9.0 m, and an outlet diameter of 80 mm. (5) A PVC pipe with a diameter of 75 cm was selected as the flow pipe. (6) A high-resolution camera (1920 × 1080 and 50 frames per second) was used as the observation system to instantaneously record the sediment incipient motion, the variation of erosion height, and the erosion duration on an actual timescale. (7) The overflow tank in the water storage tank at the top could keep the total water head constant during the test. (8) The electromagnetic flowmeter was used as the monitoring equipment for water flow rate; the flow rate range was 1.19–119 m^3/h, the measuring accuracy was ±0.01 m^3/h, and the data could be directly read from the values displayed on the electric screen.

3.2. Layout of Geogrids. The allocations of the reinforced material have been well studied previously [17, 25], so the geogrids were often laid out horizontally. When the water flows slowly along the dam body from the top to the toe, the tailings will be initiated to flow with the water overflow.

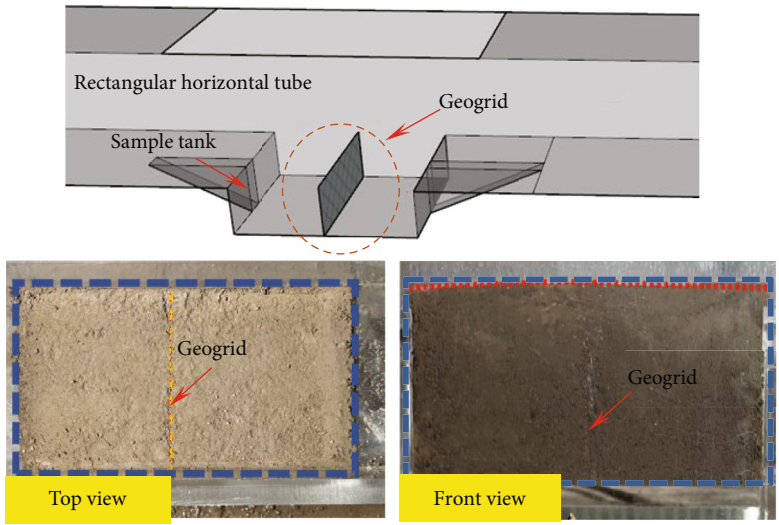

Figure 9: The layout of reinforcement-a layer of geogrid-at regional scale.

Table 3: Experimental conditions and testing results.

Test number	Red mud concentration (%)	Geogrid layers (N)	The velocity of mud-water mixture flow (cm/s)	Sample height (cm)	Final erosion depth (cm)		
					Front	Middle	Trailing end
T-1	0	N=1	19.2	4.40	1.01	0.98	0.77
T-2	10		18.7	4.34	1.17	1.04	0.61
T-3	20		18.4	4.43	1.56	0.90	0.55

When considering the frictional interaction between the geogrid and the tailings, the geogrid will have a lateral binding force on the tailings that will impact the sediment flow. As a result, a micro-segment near the geogrid was analysed and illustrated. The reinforcement layouts are illustrated in Figure 8 at both macro and local scales. In addition, the reinforcement at the regional scale was explicitly modelled, as demonstrated in Figure 9.

3.3. Erosion Behaviour in the Reinforced Fine-Grained Tailings

3.3.1. Experimental Procedures. A certain amount of tailing sample was primarily mixed with a small amount of water to achieve a gravimetric moisture content of 20%. It was then filled into the sample groove multiple times to prepare different specimens. Meanwhile, the thickness of each specimen needed to be measured to determine the bulk density of each prefabricated specimen. Subsequently, the water inlet was directed to the horizontal tube to flush each specimen's top surface along the tube bottom. Then, camera No.1 (overhead view at the top), the electromagnetic flowmeter, and camera No.2 (side view at the front) were all turned on. Afterwards, the valve was slowly opened to lead the water flow over the surface of the fine tailing specimen, so the red mud particles were dragged into the water flow to form the mud-water mixture flow (see Table 3) in the horizontal pipe flow. The water pump was also switched on to lift the water from the bottom pool to the top storage tank, in which an overflow tank was preset to ensure a constant water head. Finally, when the flow rate was increased to a critical value by slowly opening the valve, the tailing particles started to exhibit the sediment incipient motion at an initial stage and then the reading of the electromagnetic flowmeter needed to be instantaneously recorded. As for an investigation of the erosion behaviour under various red mud concentrations of mud-water mixture flow, the experiment conditions and final erosion depth are presented in Table 3.

3.3.2. Experimental Outcomes with Analysis. The erosion process on the top surface of the tailing specimen in the sample tank (the tailing dam modelled at the local scale) was varied significantly by the mud-water mixture flow, as various red mud concentrations directly affected the erosion depth. The final erosion depths of tailing specimens for different mud-water mixture flows are demonstrated in Figure 10 and quantitatively compared in Figure 11.

Figures 10 and 11 manifest that higher red mud concentrations result in relatively more apparent damage to the tailing dam model at the local scale during erosion tests. For the pure water condition (red mud concentration of 0%), the final erosion depths of the tailing specimen at the front, middle, and trailing end were 1.01 cm, 0.98 cm, and 0.77 cm, respectively. With the red mud concentration increasing, the final erosion depth of the tailing specimen increased significantly at the front, but it was reduced considerably at the trailing end. One of the primary reasons could be that the geogrid generated locking effects on the particles,

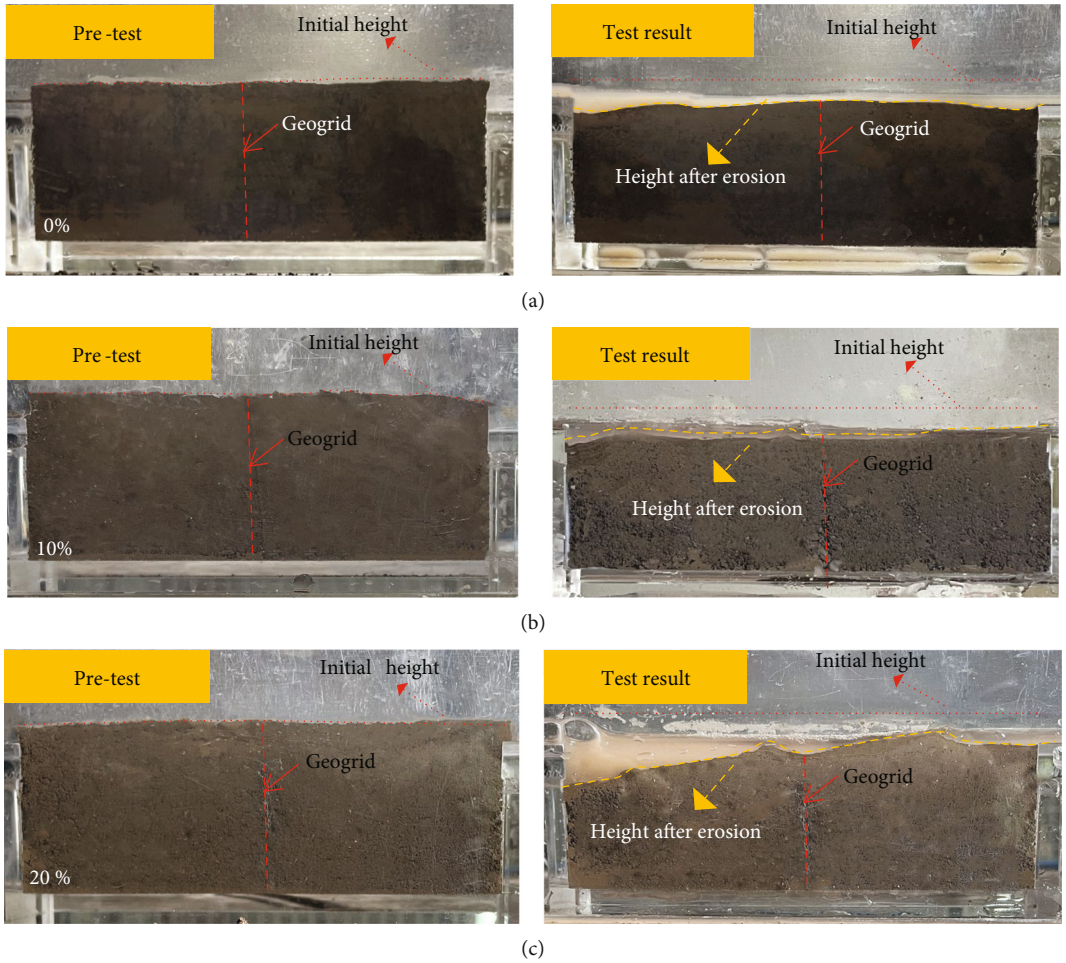

Figure 10: The erosion characterisation of the reinforced fine tailings specimen eroded by the mud-water mixture flow at the local scale for a red mud concentration of (a) 0%, (b) 10%, and (c) 20%.

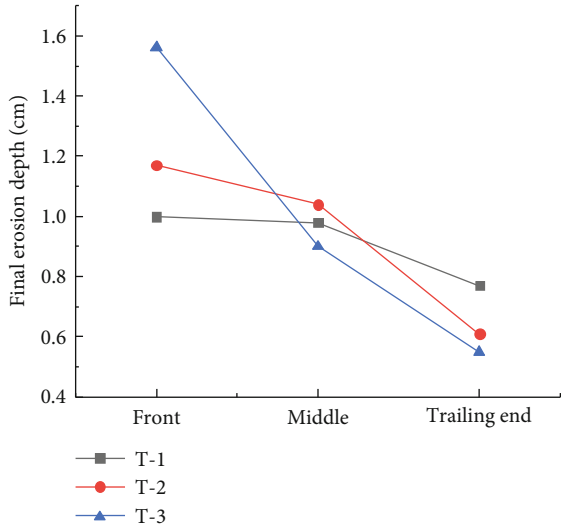

Figure 11: A comparison of erosion depths for three different red mud concentrations.

subsequently slowing down the velocity of the mud-water mixture flow. Once the erosion was impeded, the red mud particles would settle at the trailing end of the specimen.

The schematic diagram of the erosion mechanism under the mud-water mixture flow condition is shown in Figure 12. The particles in the mud-water mixture flow have enough kinetic energy. When the mud-water mixture flows to the surface of a tailing specimen, the mud particles in the water will transfer a part of the energy to the tailings, eventually causing erosion of the tailings on the surface [26]. As explained in the theory of similarity for sedimentation transport, the movement of particles can be treated as the suspended and traction loads. When the mud-water mixture flow reaches the tailing surface, some finer red mud particles are washed up by this flow, and the particles become suspended. The particles at the top surface move with the water flow and become traction load. Eventually, these two forms of movement of the particles entered the mixture flow, increasing the red mud concentration in the mixture flow. Once the settling rate in the mud-water mixture flow is higher than the mixture flow rate, the particles in the mixture flow will gradually initialise accumulation in

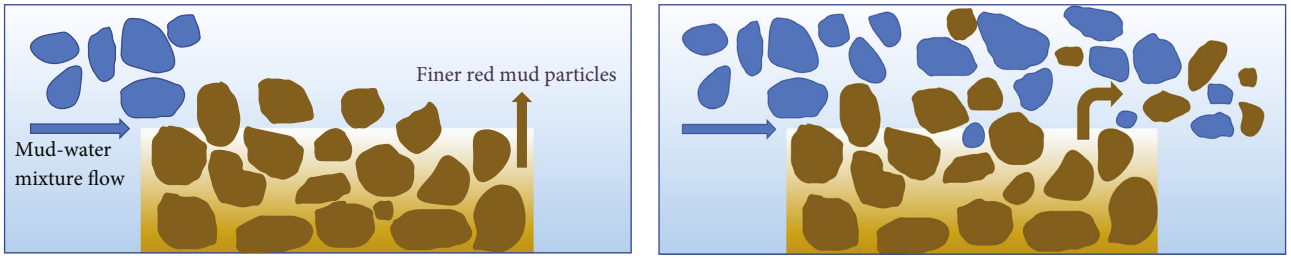

Figure 12: The schematic diagram of erosion mechanism under mud-water mixture flow: (a) an illustration of the pre-erosion process and (b) a description of the ongoing erosion process.

Table 4: Properties of the tailings.

Material	Median particle size (μm)	Density (g/cm^3)	Critical Shields number	Submarine rest angle	Bed-load transport coefficient	Entrainment coefficient
Red mud	5.1	1.8	0.0529	70°	8	0.018

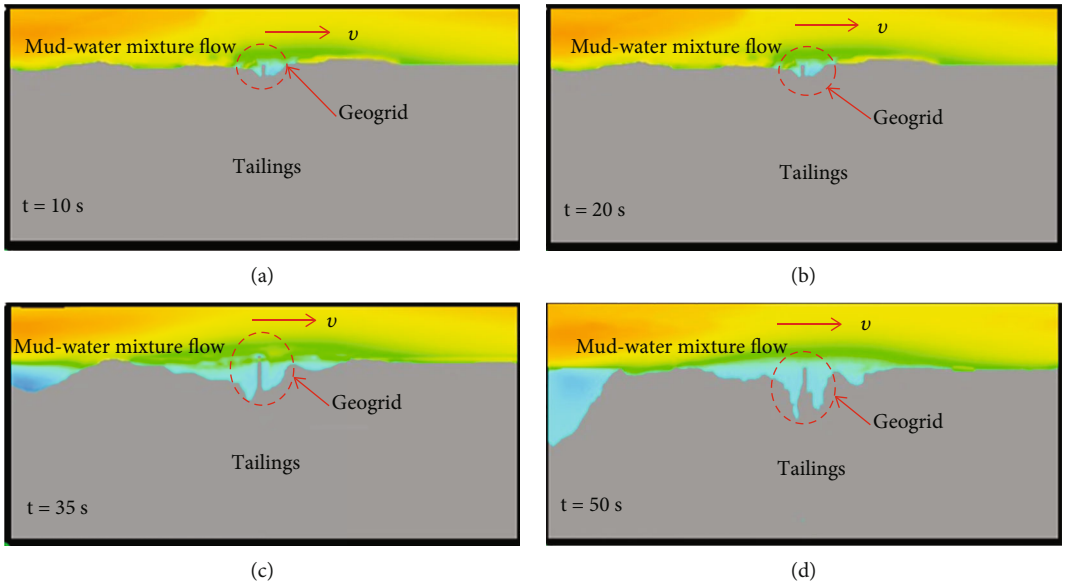

Figure 13: The cross-sectional view of erosion changes at four stages: (a) the simulation time =10 s, (b) the simulation time =20 s, (c) the simulation time =35 s, and (d) the simulation time =50 s.

the trailing end of the tailing specimen, consequently forming a pile.

4. Numerical Modelling Erosion Process on Tailing Specimen Surface

4.1. Properties of the Tailings. Red mud was used in the erosion tests, where the median particle size was 5.1 μm, and the average bulk density was 1.8 g/cm^3. The critical Shields number, the mass transition coefficient, the submarine rest angle, and other parameters referring to the work by Li et al. [27] are provided in Table 4. The numerical simulation was carried out with a red mud concentration of 10% in the mud-water mixture flow. Only a layer of geogrid was vertically embedded in the centre of simulating domain. The initial and boundary conditions were set in this numerical model according to the experimental conditions in Table 3. The simulation time was set at 50 s. The mechanism of overtopping failure has been experimentally revealed by observing the erosion process on the surface of the reinforced fine-grained tailing dam at the local scale.

4.2. Results and Analysis. After the numerical simulation was accomplished using the commercial software FLOW-3D, the Flow Sight was used to post-process the numerical outputs. Then, the simulated outcomes are shown in Figures 13 and 14. Figure 13 demonstrates that when the water flowed on the surface of the tailing specimen, the geogrid had not been

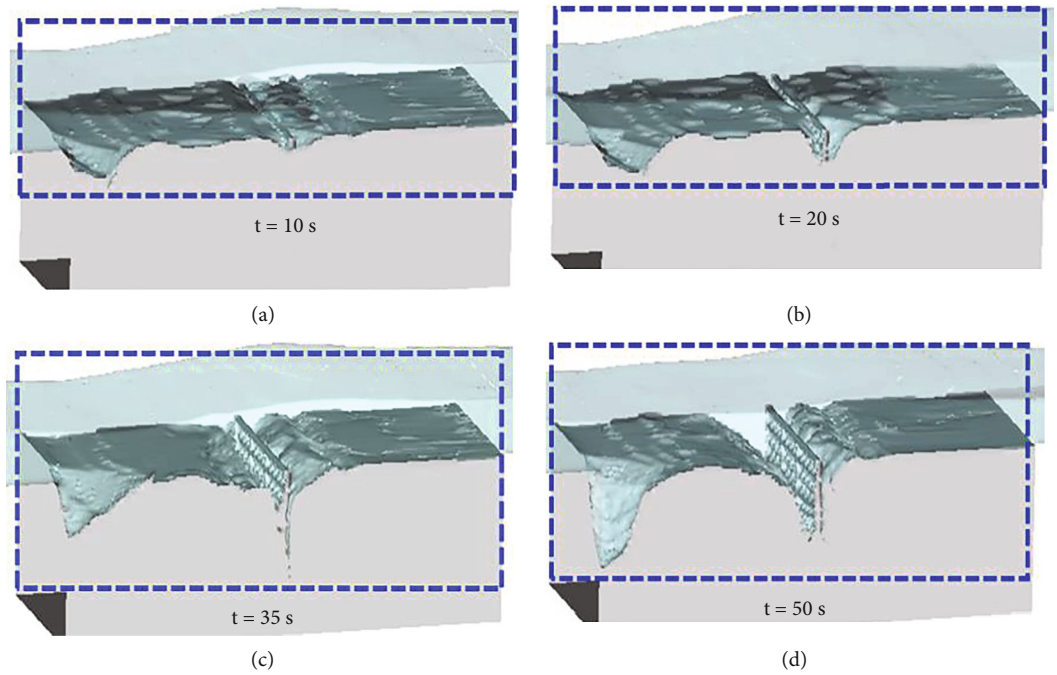

Figure 14: A series of demonstrations of the erosion destruction process at (a) the simulation time =10 s, (b) the simulation time =20 s, (c) the simulation time =35, s and (d) the simulation time =50 s.

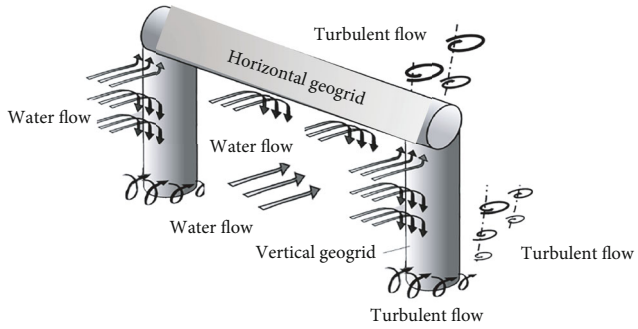

Figure 15: An illustration of the local scouring flow around the reinforcements exposed outside the tailing specimen; this part of the geogrid could be seen as a hydraulic structure, e.g., bridge piers.

exposed. The overall erosion degrees along the tailing specimen surface are similar, with a trend of relatively slight erosion. The geogrid in the middle specimen was in exposure when the numerical simulation was carried out for 10 s. Meanwhile, a pit had been gradually formed since the front of the sample was being eroded. With the simulation time increasing, the tailing specimen was more seriously eroded. Due to a particular interception effect caused by the pre-embedded geogrid, the mud-water mixture flow was transferred from the laminar flow regime to the turbulent flow regime at the local scale (see Figure 15). As a result, a small portion of the water flow penetrated the interior of the tailing specimen below the geogrid until the erosion process reached a steady state at the end of the simulation (time =50 s).

The difficulties in bending the geogrid in the testing specimen with a short exposed length can be considered a case of local erosion around the bridge piers. Thus, the local erosion theory for bridge piers was used to explain erosion characteristics in the reinforced fine-grained tailings under hydraulic loading. Figure 15 illustrates the effects of water flow around the so-defined hydraulic structure, which includes three main hydraulic features: a descending water flow, a horseshoe eddy (also named vortex), and a tailing eddy [28]. The water flow and tailings erosion caused after bypassing the longitudinal geogrid can be considered a tailing eddy behind the bridge piers. The tailings in front of the longitudinal geogrid are also eroded due to the horseshoe vortex. The water flow forms a downward flow under the influence of the horizontal geogrid. As a result, tailings erosion becomes more severe behind the geogrid because of the combined effects of those two features of the water flow.

Figures 13 and 14 show that when the water flowed through the tailings, the specimen surface became uneven rather than flat. The first erosion occurred at the front of the tailing specimen. Since the water flow gradually penetrated the tailing specimen inside, the front of the tailing specimen had been steadily eroded to form a ditch. With the water continuously flowing downstream, the water flow condition became turbulent, manifested as several eddies surrounding the geogrid. Therefore, the erosion depth in the geogrid's embedding position was higher than the thickness of the tailing specimen at the front of the geogrid and behind the geogrid.

5. Conclusions

This study has experimentally and numerically investigated the erosion characteristics of reinforced tailings dams by overtopping flows with various red mud concentrations. A series of physical modelling tests were implemented to

measure the red mud concentrations, erosion depth, and erosion rate of the overtopping flow. An experimental study of the overtopping failure caused by erosion in a reinforced fine-grained tailing dam was investigated to determine the trend in red mud concentration over time and its corresponding maximum values. The erosion damage characteristics for the reinforced fine-grained tailing specimens with three different red mud concentrations (0%, 10%, and 20%) were additionally studied using an improved experimental setup for hydraulic erosion tests at the local scale of tailing dams. The effects of reinforcement density, fine content, and red mud concentration on the erosion damage in the reinforced tailing specimens were further analysed. In addition to the physical tests, the erosion damage process was numerically simulated using FLOW-3D to illustrate the erosion mechanism with more specific details at a much smaller scale of geogrid-particle interaction. This research brought insights into the overtopping erosion of the tailing dams by the mud-water mixture overflow. All datasets and analyses presented here were applicable to reveal the erosion mechanism of the overtopping failure. Based on the experimental and numerical simulation outcomes at multiscale and research findings previously discussed, the following conclusions could be drawn:

(i) In the process of overtopping failure in tailing dams, the red mud concentration of flood along the dam slope shows a nonlinear trend in first becoming higher and then decreasing with time going on, in which the maximum red mud concentration could achieve 19.0% (the percentage (%) by mass/mass). The shape of erosion along the dam slope was like a trumpet

(ii) The red mud concentration of flow affects the erosion depth significantly. The hydraulic tests of the erosion process for the prefabricated tailing specimens with three different red mud concentrations (0%, 10%, and 20%) were implemented. As for the mud-water mixture flow with a red mud concentration of 20%, the final erosion depth had a ladder shape from the front to the trailing end of the tailing specimen. The final erosion depths were 1.56 cm, 0.9 cm, and 0.55 cm at the front, middle, and trailing end, respectively. The primary reason could be the locking effect on the tailings particle by inserting a layer of geogrid, slowing down the velocity of the mud-water mixture flow. When the erosion was impeded, the tailing was settled at the end of the tailing specimens. With the red mud concentration decreasing, the final erosion depth at the front of the tailing specimens reduced significantly while it increased at the trailing end

(iii) The erosion process was numerically explored by a commercial software FLOW-3D, which had good agreement with the experimental results at the local scale. The numerical outputs showed that with the simulation progressing to 10 s, the geogrid in the middle of the specimen was in exposures out of the specimen top. A ditch was gradually formed at the specimen front due to the eroded tailing samples. As the simulation time increased, the erosion of the tailing specimens became more and more severe and finally reached a steady state at 50 s. With the geogrid exposure deepened, the erosion on the specimen surface also increased linearly. Still, the erosion at the front of the geogrid was significantly higher than that at the rear of the geogrid, indicating that the geogrid served as a barrier

Data Availability

The data used to support the findings of this study are available from the corresponding author upon request.

Conflicts of Interest

The authors declare no conflict of interest.

Authors' Contributions

M.C. contributed to the conceptualisation; X.J. contributed to the methodology; X.H. contributed to the validation; M.C. was responsible for the supervision; X.J. and X.L. contributed to the writing—original draft preparation; X.J. and W.N. contributed to the writing—review and editing.

Acknowledgments

This research is funded by the National Natural Science Foundation of China (Grants Nos. 51974051, 51804051, and 51804222), China Occupational Safety and Health Association (CXCY-2021-19), the Self-made Equipment Foundation of Chongqing University of Science and Technology (No. ZZSB2019013), and the Graduate Innovation Program Project of Chongqing University of Science and Technology (Grants Nos. YKJCX2120702, YKJCX2120719, and YKJCX2120721).

References

[1] C. C. Chen, Y. Q. Zhao, and L. J. Jiang, "Review on the current research of dam break of tailings pond," *Mining Research and Development*, vol. 39, no. 6, pp. 103–108, 2019.

[2] L. F. Harder Jr. and J. P. Stewart, "Failure of Tapo Canyon tailings dam," *Journal of Performance of Constructed Facilities*, vol. 10, no. 3, pp. 109–114, 1996.

[3] G. E. Blight, "Destructive mudflows as a consequence of tailings dyke failures," *Proceedings of the Institution of Civil Engineers-Geotechnical Engineering*, vol. 125, no. 1, pp. 9–18, 1997.

[4] R. K. McDermott and J. M. Sibley, "The Aznalcóllar tailings dam accident — a case study," *Mineral Resources Engineering*, vol. 9, no. 1, pp. 101–118, 2000.

[5] A. Fourie, G. E. Blight, and G. Papageorgiou, "Static liquefaction as a possible explanation for the Merriespruit tailings dam failure," *Canadian Geotechnical Journal*, vol. 38, no. 4, pp. 707–719, 2001.

[6] G. Villavicencio, R. Espinace, J. Palma, A. Fourie, and P. Valenzuela, "Failures of sand tailings dams in a highly seismic country," *Canadian Geotechnical Journal*, vol. 51, no. 4, pp. 449–464, 2014.

[7] E. J. Sun, X. K. Zhang, Z. X. Li, and Y. H. Wang, "Tailings dam flood overtopping failure evolution pattern," *Procedia Engineering*, vol. 28, no. 8, pp. 356–362, 2012.

[8] Z. Z. Wu and G. D. Mei, "Statistical analysis of tailings pond accidents and cause analysis of dam failure," *China Safety Science Journal*, vol. 24, no. 9, pp. 70–76, 2014.

[9] X. Y. Lv and J. W. Teng, "Who should be responsible for this disaster: investigation of the "9.8" special major tailings dam collapse accident in Xiangfen, Shanxi Province," *Labor protection*, vol. 2008, no. 10, 2008.

[10] M. L. Yao, *Study the Mechanism of Overtopping Dam Break of Tailings Dam with Heavy Rainfall*, Chinese Master's Theses Full-text Database, 2017, http://cdmd.cnki.com.cn/Article/CDMD-10674-1017221103.htm.

[11] Y. Yang, S. Y. Cao, K. J. Yang, and W. P. Li, "Experimental study of breach process of landslide dams by overtopping and its initiation mechanisms," *Hydrodynamics Research and Progress Series B (English Edition)*, vol. 27, no. 6, pp. 872–883, 2015.

[12] J. Chen, Q. H. Jinag, C. Yao, and J. R. Niu, "Numerical simulation of dam breaks for tailing ponds," *Water resources and power*, vol. 35, no. 10, pp. 90–94, 2017.

[13] G. R. Hancock, "The use of landscape evolution models in mining rehabilitation design," *Environmental Geology*, vol. 46, no. 5, pp. 561–573, 2004.

[14] S. M. Li, L. W. Yuan, H. Yang, and G. J. Wang, "Tailings dam safety monitoring and early warning based on spatial evolution process of mud-sand flow," *Safety Science*, vol. 124, no. 4, pp. 104579–104594, 2020.

[15] X. F. Jing, X. Zhou, Y. S. Zhao, K. H. Liu, C. Ye, and C. S. Pan, "Study on the influence of reinforcement density on overtopping failure of tailings dam," *Journal of safety science and technology*, vol. 12, no. 8, pp. 68–74, 2016.

[16] Y. S. Zhao, X. F. Jing, X. Zhou, Z. Y. Cai, and K. H. Liu, "Experimental study on blocking the action of bar strip on tailings dam overtopping," *China safety science journal*, vol. 26, no. 1, pp. 94–99, 2016.

[17] P. F. Gao, J. W. Wang, H. M. Zhou, X. Cui, and X. M. Li, "Application of geotextile in the design of hillside tailings embankment," *Nonferrous Metals(Mining Section)*, vol. 71, no. 5, pp. 41–46, 2019.

[18] F. Bahmanpouri, Daliri, Khoshkonesh, Montazeri Namin, and Buccino, "Bed compaction effect on dam break flow over erodible bed; experimental and numerical modeling," *Journal of Hydrology*, vol. 594, no. 3, pp. 125645–125660, 2021.

[19] G. Petkovšek, M. A. Hassan, D. Lumbroso, and M. Roca Collell, "A two-fluid simulation of tailings dam breaching," *Mine Water and the Environment*, vol. 40, no. 1, pp. 151–165, 2020.

[20] A. R. Bagnold, "Some flume experiments on large grains but little denser than the transporting fluid, and their implications," *Ice Proceedings Engineering Divisions*, vol. 4, no. 2, pp. 174–205, 1955.

[21] H. Bruhl and I. Kazanskij, "New results concerning the influence of fine particles on sand-water flows in pipes," *Hydrotransport*, vol. B2, pp. 19–28, 1976.

[22] A. Shvidchenko and G. Pender, "Flume study of the effect of relative depth on the incipient motion of coarse uniform sediments," *Water Resources Research*, vol. 36, no. 2, pp. 619–628, 2000.

[23] H. Torfs, H. Mitchener, H. Huysentruyt, and E. Toorman, "Settling and consolidation of mud/sand mixtures," *Coastal Engineering*, vol. 29, no. 1-2, pp. 27–45, 1996.

[24] X. Zhu and X. M. Huang, "Laboratory simulating test and field settlement observation of reinforced embankment," *Chinese Journal of Geotechnical Engineering*, vol. 24, no. 3, pp. 386–388, 2002.

[25] H. W. Zhang, L. Liu, H. L. Bu, and D. Y. Zhong, "Test and design of tailings dam model," *Yellow River*, vol. 33, no. 12, pp. 1–5, 2011.

[26] J. Deng, Y. Q. Yang, H. R. Sheng, W. L. Xu, and J. W. Dong, "The influence to abrasion of sediment concentration," *Journal of sediment research*, vol. 4, no. 2000, pp. 65–68, 2000.

[27] H. K. Li, X. Liang, and H. H. Liu, "Three-dimensional numerical simulation of tailings dam failure based on FLOW-3D," *Journal of Nanchang University (Engineering & Technology)*, vol. 41, no. 2, pp. 120–126, 2019.

[28] J. L. Briaud, "Case histories in soil and rock erosion: Woodrow Wilson bridge, Brazos river meander, Normandy cliffs, and New Orleans levees," *Journal of Geotechnical and Geoenvironmental Engineering*, vol. 134, no. 10, pp. 1425–1447, 2008.